

ANALYSIS OF THE TEMPERATURE INCREASE LINKED TO THE POWER INDUCED BY RF SOURCE

A. Ibrahiem and C. Dale

France Télécom R&D DMR/IIM
38-40 rue Général Leclerc
Issy Les Moulineaux, 92794 France

W. Tabbara

SUPELEC, Département de Recherche en Electromagnétisme
Plateau de Moulon, 91192 Gif Sur Yvette, France

J. Wiart

France Télécom R&D DMR/IIM
38-40 rue Général Leclerc
Issy Les Moulineaux, 92794 France

Abstract—Temperature increase analysis has been performed with consideration to the anatomical model of the human head exposed to a cellular phone operating at 900 MHz. Four different numerical methods, in particular an implicit method based on the Alternating Direction Implicit technique (ADI), were applied to solve the Bio-Heat Equation (BHE), their advantages and limitations were compared using a canonical case. The tests performed on the latest have shown that the implicit approach is well adapted to solve this type of equations. The rise of temperature in the human head exposed to the RF emission of a mobile phone with a radiated power of 250 mW at 900 MHz was analyzed. In addition the influence of the presence of the telephone kit close to the head was discussed. The influence of different thermal parameters such as the thermal conductivity and the blood perfusion coefficient on the rise of temperature has been analyzed.

The simulation carried out showed that the maximum temperature increase in the internal tissues linked to SAR deposition does not exceed 0.1°C. We recorded a temperature difference of 1.6°C in the skin due to the presence of a switched off cellular phone, which has been confirmed by the experimental measurements performed.

1 Introduction

2 The Bio-heat Equation

2.1 The Energy Conservation Law

3 Numerical Methods and Discussion

3.1 Introduction

3.2 The Implicit Method (II)

3.3 Analysis of the Methods

4 Application to the Analysis of the Rise of Temperature Induced by a Handset

4.1 The Numerical Model of the Head

4.2 SAR Calculation

4.3 Rise of Temperature Calculation

4.3.1 Introduction

4.3.2 Influence of the Presence of the Telephone

4.3.3 Influence of the SAR

5 Conclusion

Appendix A.

Appendix B.

Appendix C.

References

1. INTRODUCTION

The fast growth of wireless telecommunication systems has induced a public concern of the hazardous health effects of electromagnetic field. For a long time this question has been studied and protective limits have been established by international organizations such as ICNIRP [1] and IEEE [2] to protect the human body from RF exposure.

The dosimetry is of particular importance to check the compliance to international limits. It is also a fundamental question for the biological research since the quality of the results is linked to the quality of the exposure assessments. The specific absorption rate (SAR in W/kg) is therefore carefully controlled in biological studies dedicated to radio frequencies using experimental and numerical approaches [3–5].

The possible rise of temperature in tissues is also an important parameter and few studies [3, 4, 6, 7] have carried out the analysis of the local rise of temperature in tissues linked to RF exposure.

In this study, the rise of temperature induced by a given SAR distribution associated with a phone emission was analyzed. The local rise of temperature is influenced by the power dissipated in the tissues but by thermal exchange via neighboring tissues and the external environment [4, 8].

The rise of temperature of a thermal model of the human head is governed by the Bio-Heat equation (BHE). This BHE models the different mechanisms of the heat-exchange such as the heat conduction, the blood flow and the metabolism. It considers also the power deposited by external sources such as those linked to the electromagnetic field.

Dealing with the exposure to handset RF emissions, the expected rise of temperature is small, hence in this study the electromagnetic dielectric and thermal properties of the tissues were not to be modified by such small increase of temperature.

The SAR in specific tissues was calculated using the Finite Difference in Time Domain (FDTD) [9]. This method is recognized as being the best approach for making these calculations and the most widely accepted computational method for SAR modeling. The frequencies used by radio cellular systems exceed hundreds of megahertz, therefore the electromagnetic fields associated are established in few nanoseconds, while the rise of temperature is achieved in few minutes. Consequently, in the bio-heat equation, the distribution of SAR in the tissues were considered to be independent of time and equal to the SAR obtained at the steady state.

The BHE [10] can be numerically solved using different explicit and implicit methods. Many studies have used the explicit form, which is easier to implement, whereas, the implicit finite difference methods [3] has not been applied intensively to solve the Bio-Heat-Equation. In this paper, our study was focused in particular on an implicit method [11], which is used for the first time to calculate the rise of temperature in the human head. We have analyzed the stability of this approach and defined a specific criterion for its stability. The advantages and limitations of these methods were checked on a canonical problem.

After this investigation, the new approach has been used to estimate the rise of temperature in the human head exposed to the emissions of a handset. The numerical model of the head was built from MRI images; it consists of 10 tissues such as skin, muscle, skull, cerebra-spinal fluid (CSF), fat, white and grey matter. The dielectric properties of these tissues were those used worldwide for SAR

calculation [12]. The mobile phone was modeled by a generic handset operating at 900 MHz and it was placed in a “cheek position” defined in international standard [13].

We have applied the FDTD on a graded mesh to estimate the SAR. The resolution in the area close to the ear was one millimeter and 3 millimeters on the opposite side of the head. E field strength and SAR were estimated in this configuration with a radiated power of 250 mW.

To conclude this study, an analysis was carried out on effects of the presence of a telephone kit close to the head (without RF emission) and the effect on the rise of temperature due to the variations in thermal parameters with regards to the existence of some uncertainties in the values of these parameters.

2. THE BIO-HEAT EQUATION

2.1. The Energy Conservation Law

The evolution and the distribution of the temperature inside the living tissues are governed by the heat-exchange such as the heat conduction, the blood flow and the metabolism. They depend also on the contribution of external sources such as the power deposited by RF sources. The partial differential equation (1) is given by [14]:

$$\begin{aligned} \rho_{(x,y,z)} C_{(x,y,z)} \frac{\partial T_{(x,y,z,t)}}{\partial t} = & \left[\nabla \cdot \left(k_{(x,y,z)} \cdot \nabla T_{(x,y,z,t)} \right) + h_{m(x,y,z)} + \rho_{(x,y,z)} \right. \\ & \left. \cdot SAR_{(x,y,z)} - B_{(x,y,z)} \cdot \left(T_{(x,y,z,t)} - T_b \right) \right] \\ & - \frac{1}{V_{ijk}} \left(h_{RAD_{(x,y,z,t)}} + h_{CONV_{(x,y,z,t)}} + h_{evap_{(x,y,z,t)}} \right) \quad (1) \end{aligned}$$

In this equation (1) $T_{(x,y,z,t)}$ is the instantaneous temperature of the tissue ($^{\circ}\text{C}$) at the point (x, y, z) and at the time t . $C_{(x,y,z)}$, $k_{(x,y,z)}$, $h_{m(x,y,z)}$ and $B_{(x,y,z)}$ are, for the tissues located at (x, y, z) , the specific heat ($\text{J/kg}\cdot^{\circ}\text{C}$), the thermal conductivity ($\text{W/m}\cdot^{\circ}\text{C}$), the metabolism of the tissue (W/m^3) and the blood perfusion parameter ($\text{W/m}^3\cdot^{\circ}\text{C}$), respectively. T_b is the blood temperature. h_{RAD} , h_{CONV} and h_{evap} are respectively the radiated, convective and evaporation heat losses from peripheral cells (W) from the peripheral [3], V is the increment of volume centered on (x, y, z) and ρ is the mass density in kg/m^3 .

The terms h_{RAD} , h_{CONV} and h_{evap} are accounted for only at the model-air interface and they represent the different effects of radiation,

convection and evaporation with respect to air. Their expressions are [3]:

$$\begin{aligned} h_{RAD} &= \varepsilon' \delta \cdot A_{eff} \left[(T_{skin} + 273)^4 - (T_{air} + 273)^4 \right] \\ h_{CONV} &= h_c \cdot A_{eff} (T_{skin} - T_{air}) \\ h_{evap} &= k_{evap} \cdot A_{eff} (P_{w,skin} - P_{w,air}) \end{aligned} \quad (2)$$

where $\delta = 5.67 \times 10^{-8} \text{ W}/(\text{m}^2 \cdot \text{K}^4)$ is the Stefan-Boltzmann constant; $\varepsilon' \approx 0.98$ the skin emissive parameter and A_{eff} the effective area radiated heat (m^2). T_{skin} the temperature of the skin ($^{\circ}\text{C}$); T_{air} the ambient air temperature and h_c the convection heat transfer = $2.7 \text{ W}/(\text{m}^2 \cdot ^{\circ}\text{C})$. The specific absorption rate is linked to the electric field strength through the relationship $SAR = \frac{\sigma |E|^2}{2\rho}$ where σ is the conductivity in (S/m), E is the electric field in V/m.

The correct description of heat transfer related to the blood flow is of extreme importance [12] since the perfusion coefficient, the heat capacity and the temperature of blood have major influences on the temperature of tissues. In this study the approach often applied [3, 4, 12] in this domain was used. This approach considers that the thermal exchange is related to the blood perfusion taking place in the smallest vessels, the blood perfusion parameter in (1), $B_{(x,y,z)}$, is therefore given by the blood specific heat multiplied by the perfusion rate [12] specific to tissues.

This study analyses the rise of temperature associated with the exposure to handset RF emissions. In this case the expected rise of temperature is small, so we have assumed that the electromagnetic dielectric and thermal properties of the tissues were assumed not to be modified by such a small increase of temperature. The SAR was therefore calculated using the dielectric properties of living tissues at the ambient temperature [15] and whilst the expected small rise of temperature was considered to have no influence on the SAR calculated.

The maximum raise in temperature (δT_{\max}) caused by the EM energy deposited (SAR) was obtained from the difference between the temperature for the exposed model to RF emissions ($SAR \neq 0$) and that of the unexposed model ($SAR = 0$) (with the telephone set still close to the head but switched off). At the equilibrium state, the small expected rise of temperature led us also to consider the metabolism and thermal properties of tissues (k, h_m, B) are non affected by the rise of temperature (δT) and independent of time.

In radio frequencies of wireless systems, the electromagnetic steady state is established in few nanoseconds whilst the rise of

temperature requires a few minutes. Therefore, in this study the specific absorption rate in the bio-heat equation was considered the SAR at a steady state. At the thermal steady state, the rise in temperature is the difference between the temperature calculated for the model exposed to the RF source, $T_{[(i,j,k,t),(SAR \neq 0)]}$, and $T_{[(i,j,k,t),(SAR=0)]}$ is the temperature for the unexposed model.

3. NUMERICAL METHODS AND DISCUSSION

3.1. Introduction

The BHE is a partial differential equation that can be solved using different numerical methods based on finite differences. Explicit Methods [4, 10, 16] and Implicit Methods [11, 16] can be used, it is of interest to analyse their advantages and limitations.

In the case of a uniform mesh grid, the accuracy is of second order in space and of first order in time (i.e., the truncation error $(TR) = O[(\Delta t), (\Delta x)^2, (\Delta y)^2, (\Delta z)^2]$). Whereas, if a non-uniform mesh grid is used, the second order accuracy in space is lost. Nevertheless, if the maximum increment ratio between two successive mesh-lines $(\Delta x_{i+1}/\Delta x_i)$ has values of the order of 1.2, then the centered difference scheme is slightly modified and the accuracy is still precise [17].

The first Explicit Method (I) is derived through a differential approach by the discretization of the BHE on an orthogonal grid that can have uniform or non-uniform spacing in any direction by applying a finite difference scheme [10, 16, 18].

With this approach, at the location $(i \delta x, j \delta y, k \delta z)$, the temperature at time step $n + 1$ is estimated using the tissues characteristics and temperature at time step n . The time step (Δt) is calculated according to the stability condition mentioned in [10].

In the second approach of the Explicit Method (II) [4, 19], a convection boundary condition is added and applied at the interface between the phantom and the surrounding media, then the terms h_{RAD} , h_{CONV} and h_{evap} in (2) are removed. The convection boundary condition leads to a new time step calculated in the absence of air and avoiding the burden of cpu time cost as mentioned in [8]. This method can be applied only with a uniform spacing between the mesh-lines $(\delta = \delta x = \delta y = \delta z)$.

The Alternating-Direction-Implicit (ADI) method (I) [16], separates the operators into one-dimensional components schemes, through three steps (for three-dimensional problems). Each step involves only the implicit operations originating from a single coordinate.

This conditionally stable method [16] allows solving iteratively the BHE with a time step 9 times larger than those of the first Explicit Method ($\Delta t_{IMPLICIT(I)} = 9 \times \Delta t_{EXPLICIT(I)}$). However, it can also be applied to the uniform and non-uniform problems. Furthermore, a system of three equations is adapted to solve the BHE listed in Appendix A.

3.2. The Implicit Method (II)

This Douglas-Rachford method [11] based on the ADI technique achieves a higher order of accuracy providing an unconditionally stable scheme [11] when applied to the heat equation in its parabolic form [10].

In order to solve these three dimensional heat conduction problems, a system of three equations listed in Appendix B [11] is used to calculate iteratively the temperature values at the three time levels $T_{i,j,k}^{n+1/3}$, $T_{i,j,k}^{n+2/3}$ and $T_{i,j,k}^{n+1}$. The resulted temperatures from the first time level equation $T_{i,j,k}^{n+1/3}$, are used as input to the second time level equation in order to calculate $T_{i,j,k}^{n+2/3}$. In the third step, the temperatures at the advanced time level $n + 1$ are computed as functions of $T_{i,j,k}^{n+1/3}$ and $T_{i,j,k}^{n+2/3}$ obtained in the first two steps. These equations can be rearranged to obtain a relation between two different time levels through a tri-diagonal matrix. We used the LU decomposition method [20] to solve the tri-diagonal system.

The stability is conditional when different parameters such as the metabolism or perfusion are taken into account. Nevertheless by applying this implicit method to solve the BHE, we can achieve very large time steps in comparison with other methods. Therefore, it is well adapted to bio-electromagnetic problems and has been used to estimate the temperature rise linked to acute radio frequency exposure.

Solving the BHE (1) by the implicit method helps analyze the influence of the different effects separately (convection, evaporation and radiation), which can not be applied using the explicit method II.

Since the stability criterion does not exist in our case, we performed a stability analysis in this application where some additional terms have had to be added to the parabolic heat equation in order to construct the BHE. The stability analysis for this implicit method is detailed in the Appendix C.

For the conditionally stable methods [4, 10, 16] mentioned in Section 3.1, their maximum time steps (Δt_{\max}) were calculated referring to the stability condition for the parabolic form of the diffusion equation.

3.3. Analysis of the Methods

The temperature rise in a canonical problem was estimated using the four methods previously mentioned. In this canonical case a half wavelength dipole antenna operating at 900 MHz is located close to a cube of material composed of layers having the same thermal properties as biological tissues (skin, bone and brain) (listed in Table 3). We performed the SAR calculation using the FDTD method with a uniform resolution of 2 mm along the three axes. The thickness of each of the both layers is equivalent to 2 cells. A maximum temperature rise close to 0.1°C is obtained by the four methods as illustrated in Figure 1.

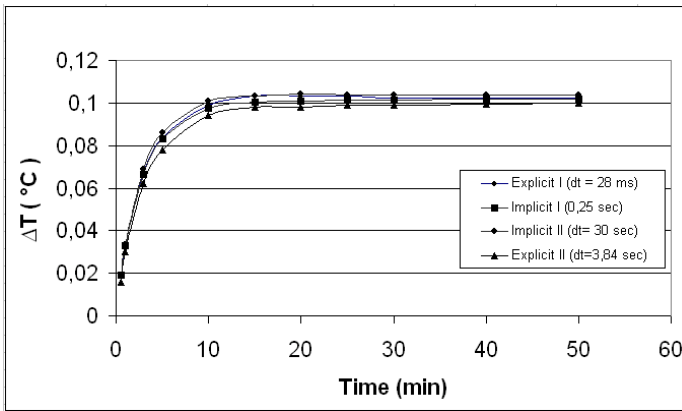


Figure 1. Comparison between the four different methods applied to the canonical test case.

The main differences are in the time step used by these methods. The time step required for the explicit method (I) was equal to 28.22 ms, whereas the time step of the explicit method (II) was equal to 3.8 sec. For the implicit method (I), the time step was equal to 0.264 s, whereas in case of applying the alternating directional implicit method (II) of Douglas and Rachford [11], a large time step can be achieved equal to 215 s, which is 7750 times larger than the first explicit method. It is worth mentioning that a maximum error of 5% was obtained when applying the implicit method (II) with a time step equal to 1 sec and 215 sec.

These results have shown that the second implicit method is well adapted to solve the BHE, therefore we have used this approach to analyze the rise of temperature induced by handset in the human tissues.

Table 1. Comparison between the perfusion coefficient (B) for the different tissues.

References Tissues	B [W/(m³·°C)]		
	[28]	[7], [8]	[18]
Skin	9100	9100	8652
Muscle	2700	2700	3488
Bone	Bone narrow = 32000	1000	1401
Grey matter	40000	35000	37822
White matter	40000	35000	37822

Table 2. Different thermal conductivity (k) values for different tissues.

References Tissues	k [W/(m·°C)]			
	[3]	[7], [8]	[19]	[12]
Skin	0.334	0.42	0.5	0.342
Muscle	0.5	0.5	0.6	0.56
Bone	0.36	0.4	0.3	0.65
Grey matter	0.528	0.57	0.6	0.565
White matter	0.528	0.5	0.6	0.503
CSF	0.57	0.6		

It is important to notice that the term $(\nabla k \cdot \nabla T)$, mentioned in Appendices (A, B), is taken in consideration when the BHE is used to solve inhomogeneous problems. If neglected, this term leads to a difference of 1% to 3% in the calculated temperature.

4. APPLICATION TO THE ANALYSIS OF THE RISE OF TEMPERATURE INDUCED BY A HANDSET

4.1. The Numerical Model of the Head

The heterogeneous human head phantom developed in the frame of the French COMOBIO project has been used to carry out this analysis. This head model has been built from magnetic resonance imaging (MRI) scans through a segmentation process. The model is composed

of 10 different tissues including skin, muscle, skull, cerebro-spinal fluid (CSF), fat, white and gray matter. The original uniform grid size was 1mm, but in order to reduce memory storage, a non-uniform meshing was selected for modeling this head. The resolution in the area close to the ear is one millimeter and is gradually increased to 3 millimeters on the opposite side of the head.

The generic handset, operating at 900 MHz, is made of a metallic box (11 cm \times 6 cm \times 3 cm) surrounded by a one-millimeter thick layer of plastic. The antenna, a quarter wavelength wire, is located at 1.4 cm from the corner of the box closest to the ear. The input power is 250 mw as it is with GSM 900 handset. The handset is lined up with the mouth and the ear and was placed in a cheek position as defined in standards [13].

The dielectric parameters, relative permittivity and conductivity, of the tissues used in the head model are based on the 4-Cole-Cole analysis [15]. The thermal conductivity, the specific heat, the blood flow rate and the metabolic heat production used in this paper are listed in Table 3.

Table 3. Thermal properties assumed for the various tissues.

Tissue	ρ [Kg/m ³]	C [J/(°C.kg)]	K [W/(m.°C)]	h_m [W/m ³]	B [W/(m ³ .°C)]
Air	1.16	1000	0.0263	0	0
Skin	1010	3500	0.42	1000	9100
Muscle	1040	3600	0.5	690	2700
Fat	920	2500	0.25	180	520
Bone	1810	1300	0.4	0	1000
Cartilage	1100	3400	0.45	1000	9100
Gray matter	1040	3700	0.57	10000	35000
White matter	1040	3600	0.5	10000	35000
Blood	1060	3900	0.51	0	0
CSF	1010	4000	0.6	0	0
Eye	1170	4200	0.58	0	0

4.2. SAR Calculation

The Specific Absorption Rate (SAR in W/kg) is the physical quantity associated with the RF power deposition in tissues linked to the electric field (see Section 2).

As explained in the introduction, the FDTD [21] often used in bio-electromagnetic studies, has become a popular tool to analyze the RF exposure [22–24].

The computational volume is truncated using the absorbing boundary conditions to simulate free space and avoid spurious reflections from the edges. In this study, we used the Perfectly Matched Layer (PML) absorbing boundary conditions, which are able to limit to less than -40 dB the spurious reflections [25, 26]. In this configuration we found the maximum value of the SAR over 10 grams equal to 0.9 W/kg. Figure 2a illustrates the spatial SAR distribution in the head.

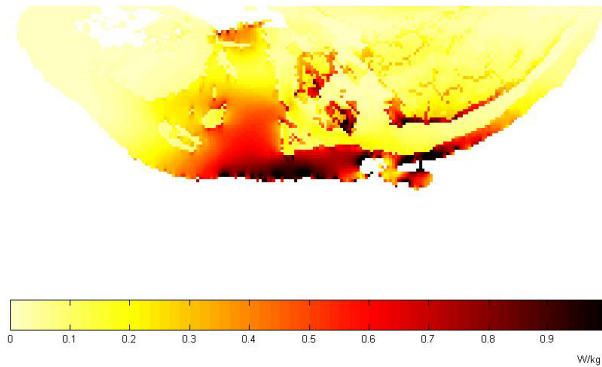


Figure 2a. Vertical cross-section of the SAR distribution in the human head [W/kg].

4.3. Rise of Temperature Calculation

4.3.1. Introduction

The presence of the telephone set close to the ear and the skin blocks the air in this region and reduces the thermal exchange with the surroundings hence the neglect of the effects of the convection, radiation and evaporation are to be taken into consideration in this region. The ambient temperature and the arterial blood temperature are assumed to be 25°C and 37°C , respectively.

The thermal response in the human head due to the exposure to the EM fields of cellular phones at 900 MHz and the heating of the pinna caused by the warm handset were studied. The various cases considered for the cellular telephone were as follows:

- a) *Case I:* The model of the human head.

- b) *Case II*: the same model as case I, but with a switched off handset (without RF emission) nearby to the left ear. This case shows the effect of the blocked air and the heating of the pinna due to the heat conduction from the handset. (Section 4.3.3).
- c) *Case III*: The same model as case II, but with the cellular phone radiating at 900 MHz with a maximum value of the SAR calculated over 10 grams and equal to 0.9 W/kg. This model has the effect of the thermal influence of the EM waves represented by the SAR (Section 4.3.2).

The implicit method II was applied with a time-step chosen to be 3.5 seconds. We have observed that in the first few minutes of calculation, the temperature rises rapidly, and more than 90% of the steady state temperature is achieved after about 10–15 min of RF emission, the rate of the temperature rise slows down and the steady state temperature obtained in the ear region is equal to 0.08°C after approximately 50 min of exposure as shown in Figure 2b. These results show that the maximum temperature rise is less than 0.1°C in the skin, which agrees with the previous studies [3, 4, 8, 19].

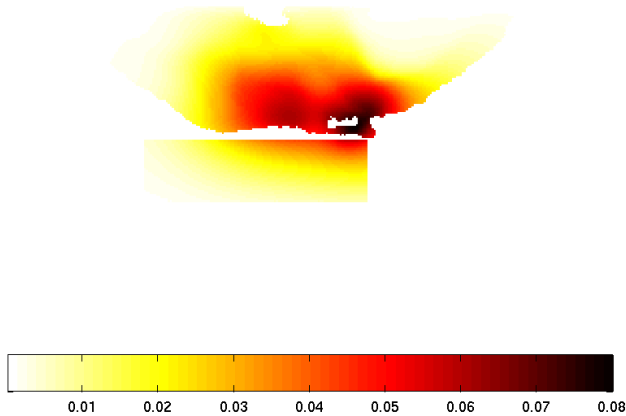


Figure 2b. Rise of temperature in the model of the human head.

We carefully analysed these different cases separately, the influences of the SAR and the telephone set on the increase of temperature as follows are shown as below:

4.3.2. Influence of the Presence of the Telephone

In order to study the thermal effect resulted from the presence of a switched off cellular telephone handset close to the head (without RF emission), we calculate the temperature in “*case I*” at the equilibrium state, then we added the turned off handset considered to be at initial temperature of 25°C, against the left ear. It is important to note that during the first few minutes, the handset temperature started to increase simultaneously with a decrease in the skin temperature whilst the steady state was reached after 20–30 minutes.

A maximum difference of temperature of 1.6°C was obtained by the numerical simulations as shown in Figure 3. This result has been confirmed by using a LUXTRON fiber optic thermometer to measure the skin temperature in the ear region covered by the handset.

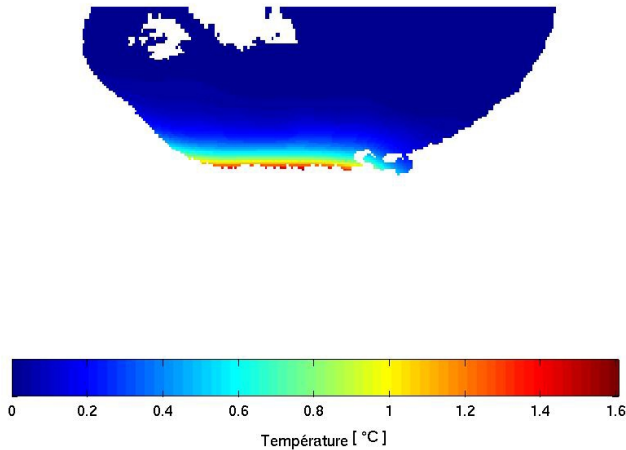


Figure 3. The influence of the telephone set on the human head.

4.3.3. Influence of the SAR

The rise of temperature ($\Delta T_{(i,j,k)}$) due to the RF exposure of a cellular phone is difference between the temperature of the exposed head, $T_{[(i,j,k,t),(SAR \neq 0)]}$, and $T_{[(i,j,k,t),(SAR=0)]}$ where $T_{[(i,j,k,t),(SAR=0)]}$ is the temperature for the unexposed head at the thermal equilibrium. The obtained results show that the maximum temperature in the internal tissues is around 0.08°C but does not exceed 0.1°C. It is worth

mentioning that the simulations show that the peak of SAR occurs in the skin (Figure 2a), whilst the peak temperature rise occurs in the ear region (Figure 4).

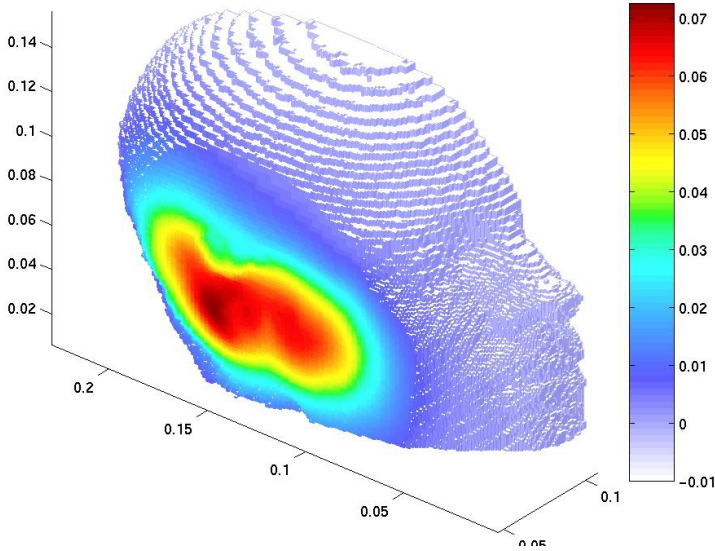


Figure 4. Maximum rise of temperature in the human head after exposure duration of 50 min.

4.3.3.1. Rise of temperature in specific tissues

A maximum temperature rise of 0.06C was obtained in the brain region and it was observed that the maximum rise of temperature in the head appears on the skin and in its neighboring region. (Table 5) list the maximum temperature values calculated in the different tissues of the human head.

4.3.3.2. Influence of parameters

The analysis of thermal characteristics of the head tissues used in the literature [12, 19, 7] shows large variations in their values. Therefore it is of interest to study the maximum variations in the rise of temperature caused by the variation in the different thermal parameters. Furthermore, the effect of the convection is important for investigation, hence so this effect was taken in consideration in this study.

As shown in Table 1 and Table 2, an average change of $\pm 30\%$

Table 4. Maximum rise of temperature caused by the different parameters (in °C). (a) The heat capacity C . (b) The thermal conductivity. (c) The coefficient associated to the blood perfusion.

C	$\Delta T_{(+30\%)} (^{\circ}\text{C})$	$\Delta T_{(-30\%)} (^{\circ}\text{C})$
Ear and skin	0.08	0.08
Brain	0.06	0.06
Bone	0.07	0.07

(a)

k	$\Delta T_{(+30\%)} (^{\circ}\text{C})$	$\Delta T_{(-30\%)} (^{\circ}\text{C})$
Ear and skin	0.07	0.09
Brain	0.05	0.06
Bone	0.06	0.08

(b)

B	$\Delta T_{(+30\%)} (^{\circ}\text{C})$	$\Delta T_{(-30\%)} (^{\circ}\text{C})$
Ear and skin	0.06	0.09
Brain	0.04	0.06
Bone	0.06	0.08

(c)

was assumed for the variation of each of the thermal parameters (k , B , C) of the tissues (skin, brain and bone), in order to investigate the maximum temperature rise. The maximum temperature rise rates of the skin and the brain were 0.08°C and 0.06°C , respectively. As seen from Table 4, the maximum variation in temperature obtained was 15% when the blood coefficient (B) changed by $\pm 30\%$ for all the tissues. A 10% can be caused by a variation of $\pm 30\%$ in the thermal conductivity for the different tissues. The main effect caused by the variation in heat capacity (C) is the variation in the time constant of the heat conduction.

In order to investigate the effect of the convection, we compared the results obtained in the case of neglecting the convection coefficient ($h_c = 0$) with the original results calculated when ($h_c \neq 0$). At the thermal steady state, we recorded a maximum difference of 1% between the two cases.

Table 5. Maximum temperature calculated in the different tissues of the human head.

Tissues	ΔT ($^{\circ}\text{C}$)
Ear and skin	0.08
Brain	0.06
Bone	0.07

5. CONCLUSION

In this paper, four different numerical methods were applied to solve the BHE, their advantages and limitations are discussed. The explicit method is quite easy to implement but it is time consuming; due to a time step of only few ms. The application of the convection boundary conditions in the second explicit method at air-model interface allows having an acceptable time step by neglecting the presence of air in the model. The implicit methods are more complex to implement since there is a matrix inversion, but give a good accuracy. The benefit is of real importance with the implicit method (II), whose run time is linearly proportional to the number of grid nodes [27]. Furthermore, the stability analysis of this implicit method was studied in case of the BHE. Hence, the steady state temperature is achieved after only few iterations in comparison with a more numerous number of iterations required by the other methods.

The temperature rise in the human head caused by cellular phones has been computed with an anatomically human-head model. The SAR in the human head has been determined using the FDTD method, and the bio heat equation has been numerically solved using different numerical methods; their advantages and limitations were compared. With antenna output power of 250 mW at 900 MHz, the maximum temperature rise in the skin and the brain is found to be 0.08°C and 0.06°C , respectively.

The numerical simulation shows that a cellular telephone (without emission) close to the head, increases the normal skin's temperature by a 1.6°C , which is larger than the rise of temperature caused by the power deposition in tissues.

The influence of the different effects such as the physical parameters (k , C), the blood perfusion and the convection effects which differ among various authors have been analyzed in this paper. The obtained results show the importance effect of the blood perfusion

coefficient and the thermal conductivity on the temperature rise. It should be noted that the main effect observed by the change in the specific heat is the variation in the time constant of the heat conduction.

APPENDIX A.

The Alternating-Direction-Implicit Method (I) (conditionally stable) applied for the homogenous media:

Step 1:

$$\left(\frac{T_{ijk}^{n+\frac{1}{3}} - T_{ijk}^n}{\Delta t/3} \right) = \frac{k_{ijk}}{\rho_{ijk} \cdot C_{ijk}} \cdot \left(\frac{T_{i+1,j,k}^{n+\frac{1}{3}} - 2 \cdot T_{ijk}^{n+\frac{1}{3}} + T_{i-1,j,k}^{n+\frac{1}{3}}}{\Delta x^2} + \frac{T_{i,j+1,k}^n - 2 \cdot T_{ijk}^n + T_{i,j-1,k}^n}{\Delta y^2} + \frac{T_{i,j,k+1}^n - 2 \cdot T_{ijk}^n + T_{i,j,k-1}^n}{\Delta z^2} + \frac{h_m + B_{ijk} \cdot (T_b - T_{ijk}^n)}{k_{ijk}} \right) + \frac{1}{\rho_{ijk} \cdot C_{ijk}} \cdot \left(\begin{array}{l} \nabla k_x \cdot \nabla T_x + \\ \nabla k_y \cdot \nabla T_y + \\ \nabla k_z \cdot \nabla T_z \end{array} \right) - \frac{1}{m_{ijk} \cdot C_{ijk}} \left(h_{RAD_{ijk}} + h_{CONV_{ijk}} + h_{evap_{ijk}} \right) + \frac{SAR_{ijk}}{C_{ijk}}$$

Step 2:

$$\left(\frac{T_{ijk}^{n+\frac{2}{3}} - T_{ijk}^{n+\frac{1}{3}}}{\Delta t/3} \right) = \frac{k_{ijk}}{\rho_{ijk} \cdot C_{ijk}} \cdot \left(\frac{T_{i+1,j,k}^{n+\frac{1}{3}} - 2 \cdot T_{ijk}^{n+\frac{1}{3}} + T_{i-1,j,k}^{n+\frac{1}{3}}}{\Delta x^2} + \frac{T_{i,j+1,k}^{n+\frac{2}{3}} - 2 \cdot T_{ijk}^{n+\frac{2}{3}} + T_{i,j-1,k}^{n+\frac{2}{3}}}{\Delta y^2} + \frac{T_{i,j,k+1}^{n+\frac{1}{3}} - 2 \cdot T_{ijk}^{n+\frac{1}{3}} + T_{i,j,k-1}^{n+\frac{1}{3}}}{\Delta z^2} + \frac{h_m + B_{ijk} \cdot (T_b - T_{ijk}^n)}{k_{ijk}} \right)$$

$$\begin{aligned}
& + \frac{1}{\rho_{ijk} \cdot C_{ijk}} \cdot \begin{pmatrix} \nabla k_x \cdot \nabla T_x + \\ \nabla k_y \cdot \nabla T_y + \\ \nabla k_z \cdot \nabla T_z \end{pmatrix} \\
& - \frac{1}{m_{ijk} \cdot C_{ijk}} \left(h_{RAD_{ijk}} + h_{CONV_{ijk}} + h_{evap_{ijk}} \right) + \frac{SAR_{ijk}}{C_{ijk}}
\end{aligned}$$

Step 3:

$$\begin{aligned}
\left(\frac{T_{ijk}^{n+1} - T_{ijk}^{n+\frac{2}{3}}}{\Delta t/3} \right) &= \frac{k_{ijk}}{\rho_{ijk} \cdot C_{ijk}} \cdot \begin{pmatrix} \frac{T_{i+1,j,k}^{n+\frac{2}{3}} - 2 \cdot T_{ijk}^{n+\frac{2}{3}} + T_{i-1,j,k}^{n+\frac{2}{3}}}{\Delta x^2} + \\ \frac{T_{i,j+1,k}^{n+\frac{2}{3}} - 2 \cdot T_{ijk}^{n+\frac{2}{3}} + T_{i,j-1,k}^{n+\frac{2}{3}}}{\Delta y^2} + \\ \frac{T_{i,j,k+1}^{n+1} - 2 \cdot T_{ijk}^{n+1} + T_{i,j,k-1}^{n+1}}{\Delta z^2} + \\ \frac{h_m + B_{ijk} \cdot (T_b - T_{ijk}^n)}{k_{ijk}} \end{pmatrix} \\
& + \frac{1}{\rho_{ijk} \cdot C_{ijk}} \cdot \begin{pmatrix} \nabla k_x \cdot \nabla T_x + \\ \nabla k_y \cdot \nabla T_y + \\ \nabla k_z \cdot \nabla T_z \end{pmatrix} \\
& - \frac{1}{m_{ijk} \cdot C_{ijk}} \left(h_{RAD_{ijk}} + h_{CONV_{ijk}} + h_{evap_{ijk}} \right) + \frac{SAR_{ijk}}{C_{ijk}}
\end{aligned}$$

APPENDIX B.

The Implicit Method (II) (*Douglas-Rachford Method*) applied for the homogenous media:

Step 1:

$$\left(\frac{T_{i,j,k}^{n+\frac{1}{3}} - T_{i,j,k}^n}{\Delta t} \right) = \frac{k_{ijk}}{\rho_{ijk} \cdot C_{ijk}} \cdot \begin{pmatrix} \frac{T_{i+1,j,k}^{n+\frac{1}{3}} - 2 \cdot T_{i,j,k}^{n+\frac{1}{3}} + T_{i-1,j,k}^{n+\frac{1}{3}}}{\Delta x^2} + \\ \frac{T_{i,j+1,k}^n - 2 \cdot T_{i,j,k}^n + T_{i,j-1,k}^n}{\Delta y^2} + \\ \frac{T_{i,j,k+1}^n - 2 \cdot T_{i,j,k}^n + T_{i,j,k-1}^n}{\Delta z^2} + \\ \frac{h_m + B_{ijk} \cdot (T_b - T_{ijk}^n)}{k_{ijk}} \end{pmatrix}$$

$$\begin{aligned}
 & + \frac{1}{\rho_{ijk} \cdot C_{ijk}} \cdot \left(\begin{array}{l} \nabla k_x \cdot \nabla T_x + \\ \nabla k_y \cdot \nabla T_y + \\ \nabla k_z \cdot \nabla T_z \end{array} \right) \\
 & - \frac{1}{m_{ijk} \cdot C_{ijk}} \left(h_{RAD_{ijk}} + h_{CONV_{ijk}} + h_{evap_{ijk}} \right) + \frac{SAR_{i,j,k}}{c_{i,j,k}}
 \end{aligned}$$

Step 2:

$$\begin{aligned}
 \frac{\left(T_{i,j,k}^{n+\frac{2}{3}} - T_{i,j,k} \right)}{\Delta t} & = \frac{k_{ijk}}{\rho_{ijk} \cdot C_{ijk}} \cdot \left(\begin{array}{l} \frac{T_{i+1,j,k}^{n+\frac{1}{3}} - 2 \cdot T_{i,j,k}^{n+\frac{1}{3}} + T_{i-1,j,k}^{n+\frac{1}{3}}}{\Delta x^2} + \\ \frac{T_{i,j+1,k}^{n+\frac{2}{3}} - 2 \cdot T_{i,j,k}^{n+\frac{2}{3}} + T_{i,j-1,k}^{n+\frac{2}{3}}}{\Delta y^2} + \\ \frac{T_{i,j,k-1}^n - 2 \cdot T_{i,j,k}^n + T_{i,j,k+1}^n}{\Delta z^2} + \\ \frac{h_m + B_{ijk} \cdot (T_b - T_{ijk}^n)}{k_{ijk}} \end{array} \right) \\
 & + \frac{1}{\rho_{ijk} \cdot C_{ijk}} \cdot \left(\begin{array}{l} \nabla k_x \cdot \nabla T_x + \\ \nabla k_y \cdot \nabla T_y + \\ \nabla k_z \cdot \nabla T_z \end{array} \right) \\
 & - \frac{1}{m_{ijk} \cdot C_{ijk}} \left(h_{RAD_{ijk}} + h_{CONV_{ijk}} + h_{evap_{ijk}} \right) + \frac{SAR_{i,j,k}}{c_{i,j,k}}
 \end{aligned}$$

Step 3:

$$\begin{aligned}
 \frac{\left(T_{i,j,k}^{n+1} - T_{i,j,k}^n \right)}{\Delta t} & = \frac{k_{ijk}}{\rho_{ijk} \cdot C_{ijk}} \cdot \left(\begin{array}{l} \frac{T_{i+1,j,k}^{n+\frac{1}{3}} - 2 \cdot T_{i,j,k}^{n+\frac{1}{3}} + T_{i-1,j,k}^{n+\frac{1}{3}}}{\Delta x^2} + \\ \frac{T_{i,j+1,k}^{n+\frac{2}{3}} - 2 \cdot T_{i,j,k}^{n+\frac{2}{3}} + T_{i,j-1,k}^{n+\frac{2}{3}}}{\Delta y^2} + \\ \frac{T_{i,j,k+1}^{n+1} - 2 \cdot T_{i,j,k}^{n+1} + T_{i,j,k-1}^{n+1}}{\Delta z^2} + \\ \frac{h_m + B_{ijk} \cdot (T_b - T_{ijk}^n)}{k_{ijk}} \end{array} \right) \\
 & + \frac{1}{\rho_{ijk} \cdot C_{ijk}} \cdot \left(\begin{array}{l} \nabla k_x \cdot \nabla T_x + \\ \nabla k_y \cdot \nabla T_y + \\ \nabla k_z \cdot \nabla T_z \end{array} \right)
 \end{aligned}$$

$$-\frac{1}{m_{ijk} \cdot C_{ijk}} \left(h_{RAD_{ijk}} + h_{CONV_{ijk}} + h_{evap_{ijk}} \right) + \frac{SAR_{i,j,k}}{c_{i,j,k}}$$

APPENDIX C.

The three steps for this implicit method can be expressed in the following form as [27]:

Step 1:

$$\left(1 - r_x \cdot \delta_x^2\right) T^{n+\frac{1}{3}} = \left(1 + r_y \delta_y^2 + r_z \delta_z^2 + r_x \delta_x + r_y \delta_y + r_z \delta_z + \gamma\right) T^n \quad (C1)$$

$$\text{Step 2: } \left(1 - r_y \cdot \delta_y^2\right) T^{n+\frac{2}{3}} = T^{n+\frac{1}{3}} - r_y \delta_y^2 \cdot T^n \quad (C2)$$

$$\text{Step 3: } \left(1 - r_z \cdot \delta_z^2\right) T^{n+1} = T^{n+\frac{2}{3}} - r_z \delta_z^2 \cdot T^n \quad (C3)$$

where γ contains the different effects for the blood, radiation and the convection and $\delta_x^2 \cdot T^n = T_{i+1,j,k}^n - 2 \cdot T_{i,j,k}^n + T_{i-1,j,k}^n$, $r_x = \alpha \cdot \Delta t / (\Delta x)^2$. A similar process can be applied to the y and z directions.

By writing equation (C3) as a function of T^n , we get the following equation:

$$T^{n+1} = \left[\frac{\left(1 + r_y \cdot \delta_y^2 + r_z \cdot \delta_z^2 + r_x \cdot \delta_x + r_y \cdot \delta_y + r_z \cdot \delta_z + \gamma\right)}{\left(1 - r_z \cdot \delta_z^2\right) \cdot \left(1 - r_y \cdot \delta_y^2\right) \cdot \left(1 - r_x \cdot \delta_x^2\right)} \cdot T^n \right] \\ - \frac{r_y \cdot \delta_y^2}{\left(1 - r_z \cdot \delta_z^2\right) \cdot \left(1 - r_y \cdot \delta_y^2\right)} \cdot T^n - \frac{r_z \cdot \delta_z^2}{\left(1 - r_z \cdot \delta_z^2\right)} \cdot T^n$$

In order to check the stability of the ADI method, we have applied the discrete Fourier transform on the last three equations (C1)–(C3) to obtain:

$$T^{n+1} = \left[\frac{\left(\begin{array}{l} 1 - 2 \cdot r_y \cdot (1 - \cos k_y) - 2 \cdot r_z \cdot (1 - \cos k_z) \\ + 2 \cdot r_x \cdot \cos k_x + 2 \cdot r_y \cdot \cos k_y + 2 \cdot r_z \cdot \cos k_z + \gamma \end{array} \right)}{\left(\begin{array}{l} (1 + 2 \cdot r_z \cdot (1 - \cos k_z)) \cdot (1 + 2 \cdot r_y \cdot (1 - \cos k_y)) \\ \cdot (1 + 2 \cdot r_x \cdot (1 - \cos k_x)) \end{array} \right)} \cdot T^n \right] \\ + \frac{2 \cdot r_y \cdot (1 - \cos k_y)}{\left(1 + 2 \cdot r_z \cdot (1 - \cos k_z)\right) \cdot \left(1 + 2 \cdot r_y \cdot (1 - \cos k_y)\right)} \cdot T^n \\ + \frac{2 \cdot r_z \cdot (1 - \cos k_z)}{\left(1 + 2 \cdot r_z \cdot (1 - \cos k_z)\right)} \cdot T^n$$

The above equations can be written in a simpler form if we let

$$X = 2 \cdot r_x \cdot (1 - \cos k_x), \quad Y = 2 \cdot r_y \cdot (1 - \cos k_y), \quad Z = 2 \cdot r_z \cdot (1 - \cos k_z)$$

$$2r_x - X = 2 \cdot r_x \cdot \cos k_x, \quad 2r_y - Y = 2 \cdot r_y \cdot \cos k_y, \quad 2r_z - Z = 2 \cdot r_z \cdot \cos k_z$$

Then we get:

$$\frac{1 + (XY + YZ + XZ + XYZ) - X - Y - Z + \xi + \gamma}{1 + (XY + YZ + XZ + XYZ) + X + Y + Z}$$

Therefore, this implicit method is unconditionally stable when it is applied to homogenous problems $\xi = 0$ (ξ represent the effect of the term $\nabla k \cdot \nabla T$) and when the parabolic equation is considered without any of the additional terms considered in the BHE ($\gamma = 0$).

In case of solving the BHE, the next condition must be valid in order to remain in the stability limits: $r_x + r_y + r_z + \frac{k}{2} < X + Y + Z$.

REFERENCES

1. ICNIRP Guidelines, "Guidelines for limiting exposure to time-varying electric, magnetic, and electromagnetic fields (up to 300 GHz)," *Health Phys.*, Vol. 74, No. 4, 494–522, 1998.
2. IEEE Standard for Safety Levels with Respect to Human Exposure to Radio Frequency Electromagnetic Fields, 3 kHz to 300 GHz, IEEE standard C95.1-1991, 1992.
3. Gandhi, O. P., Q.-X. Li, and G. Kang, "Temperature rise for the human head for cellular telephones and for peak SARs prescribed in safety guidelines," *IEEE Trans. Microwave Theory Tech.*, Vol. 49, No. 9, Sept. 2001.
4. Bernardi, P., M. Cavagnaro, S. Pisa, and E. Piuzzi, "SAR distribution and temperature increase in an anatomical model of the human eye exposed to the field radiated by the user antenna in a wireless LAN," *IEEE Trans. Microwave Theory Tech.*, Vol. 46, No. 12, Dec. 1998.
5. Wiart, J. and R. Mittra, "Calculation of the power absorbed by tissues in case of hand set mobile antenna close to biological tissue," *Proc. IEEE Symp. Antennas Propagat.*, 1104–1107, Baltimore, MD, July 1996.
6. Bernardi, P., M. Cavagnaro, S. Pisa, and E. Piuzzi, "Power absorption and temperature elevations induced in the human head by a dual-band monopole-helix antenna phone," *IEEE Trans. Microwave Theory Tech.*, Vol. 49, No. 12, Dec. 2001.

7. Hirata, A., M. Morita, and T. Shiozawa, "Temperature increase in the human head due to a dipole antenna at microwave frequencies," *IEEE Trans. EMC*, Vol. 45, No. 1, Feb. 2003.
8. Bernardi, P., M. Cavagnaro, S. Pisa, and E. Piuzzi, "Specific absorption rate and temperature increases in the head of a cellular-phone user," *IEEE Trans. Microwave Theory Tech.*, Vol. 48, No. 7, July 2000.
9. Taflove, A., *Computational Electrodynamics: The Finite-Difference Time-Domain Method*, Artech House, Norwood, MA, 1995.
10. Euvrard, D., "Résolution numérique des équations aux dérivées partielles," collection Masson, 58–61, 1994.
11. Brian, P. L. T., "A finite-difference method of high-order accuracy for the solution of three-dimensional transient heat conduction problem," *Amer. Inst. Chem. Eng. J.*, Vol. 7, No. 3, 367–370, 1961.
12. Van Leeuwen, G. M. J., J. J. W. Lagendijk, B. J. A. M. Van Leersum, A. P. M. Zwamborn, S. N. Hornsleth, and A. N. T. J. Kotte, "Calculation of change in brain temperatures due to exposure to a mobile phone," *Phys. Med. Bio.*, Vol. 44, 2367–2379, PII: S0031-9155(99)02701-3, 1999.
13. CENELEC, European standard EN 50360 & EN 50361.
14. Bronzino, J. D., *Biomedical Engineering Handbook*, Vol. 1, Chapter 4, Trinity College, West Hartford, Connecticut, USA, 1999.
15. Gabriel, C., "Compilation of the dielectric properties of body tissues at RF and microwave frequencies," Occupational and Environmental Health Directorate, Brooks Air Force Technical Report AL/OE-TR-1996-0037.
16. Ozisik, M. N., *Finite Difference Methods in Heat Transfer*, 1994.
17. Chebolu, S. R. S., "Efficient modeling of passive electronic devices using the finite difference time domain method," 10, Thesis, University of Illinois at Urbana-Champaign, 1996.
18. Chatterjee, I. and O. P. Gandhi, "An inhomogeneous thermal block model of man for the electromagnetic environment," *IEEE Trans. Biomed. Eng.*, Vol. BME-30, No. 11, Nov. 1983.
19. Wang, J. and O. Fujiwara, "FDTD computation of temperature rise in the human head for portable telephone," *IEEE Trans. Microwave Theory Tech.*, Vol. 47, No. 8, Aug. 1999.
20. Press, W. H., B. P. Flannery, S. A. Teukolsky, and W. T. Vetterling, *Numerical Recipes in C*, Cambridge University, New York,

- NY, 1988.
21. Yee, K. S., "Numerical solution of initial boundary value problems involving Maxwell's equations in isotropic media," *IEEE Trans. Antennas and Propagation*, Vol. 14, No. 3, 302–307, 1966.
 22. Burkhardt, M., K. Pokovic, M. Gnos, T. Schmid, and N. Kuster, "Numerical and experimental dosimetry of Petri dish exposure setups," *Journal of Bioelectromagnetics Society*, Vol. 17, 483–493, 1996.
 23. Laval, L., Ph. Leveque, and B. Jecko, "A new in vitro exposure device for the mobile frequency of 900 MHz," *Journal of Bioelectromagnetics Society*, Vol. 21, 255–263, 2000.
 24. Watanabe, S., M. Taki, and O. Fujiwara, "Characteristics of the SAR distribution in a head exposed to electromagnetic fields radiated by a hand-held portable radio," *IEEE Trans. Microwave Theory Tech.*, Vol. 44, 1874–1883, 1996.
 25. Gedney, S. D., "An anisotropy perfectly matched layer absorbing media for the truncation of FDTD lattices," *IEEE Trans. Antennas and Propagation*, Vol. 44, 1630–1639, 1996.
 26. Berenger, J. P., "A perfectly matched layer for the absorption of electromagnetic waves," *J. Computational Physics*, Vol. 114, No. 2, 195–200, 1994.
 27. Wang, T.-Y. and C. C.-P. Chen, "3-D thermal-ADI: A linear-time chip level transient thermal simulator," *IEEE Trans. on Computer-Aided Design of Integrated Circuits and Systems*, Vol. 21, Issue 12, 1434–1445, Dec. 2002.
 28. Bernardi, P., M. Cavagnaro, S. Pisa, and E. Piuze, "Specific absorption rate and temperature elevation in a subject exposed in the far field of radio-frequency source operating in the 10–900 MHz range," *IEEE Trans. On Biomedical Eng.*, Vol. 50, No. 3, March 2003.

Ahmed Ibrahim born in Toulouse, France, in 1977. He received the B.S. degree in telecommunication from the Alexandria University, Alexandria, Egypt, in 2000, the M.S. degree in electrical engineering from the University of Paris VI in 2001 and is currently working toward the Ph.D. degree.

Christian Dale was born in Strasbourg, France, in 1973. He received his Engineer degree from the Ecole Nationale Supérieure des Télécommunications in 1996, studying computer science, networks and image processing technologies. He joined the CNET, research center of

France Telecom in 1997 working on the interactions of radiofrequencies with the human being and the electromagnetic compatibility of medical and hospital devices. Since October 1999, he is a leader of a project dealing with these matters. His research interests include image processing, bio-electromagnetics, antenna measurement and simulation and computational electromagnetic tools.

Walid Tabbara born in Beirut (Lebanon) in 1946, he obtained the Doctorat ès Sciences (Ph.D.) from the University of Paris VI in 1976. He is a Full-Professor at the same university since 1981. His research is done at the Département de Recherche en Électromagnétisme (DRE) of Supélec. From 1987 to 1996 he acted as a Deputy Director of the Laboratoire des Signaux et Systèmes (Supélec-CNRS). From 1984 to 1990 he acted as the french delegate to commission B of URSI. He is a member of URSI, the Electromagnetics Academy and, the editorial boards of the Journal of Electromagnetic Waves and Applications (JEWA) and of the Journal of Computer Applications in Engineering Education. He organized and/or chaired sessions at national and international conferences. After working for a long period in the field of inverse scattering in electromagnetics and acoustics, his present fields of interest are Electromagnetic Compatibility (EM, remote sensing, indoor propagation and High Power Microwaves (HPM). His present and passed researches has led to the publication of 48 papers in international journals and to 158 presentations at international and national conferences.

Joe Wiart received the Engineer degree from the Ecole Nationale Supérieure des Telecommunication, Paris France, in 1992 and the Ph.D. degree in physics from the ENST and P&M Curie University, Paris, France in 1995. He joined the CNET – the Research Center of France Telecom in 1992 and spent three years working on propagation in micro cellular environment. Since 1994 he has been working on the interaction of radiowaves with the human body and on medical electronic devices. He is currently the head of a group dealing with these questions in CNET. His research interests include EMC, bio-electromagnetics, antenna measurements, computational electromagnetics and signal processing. Dr. Wiart is Vice Chairman of the COST 244 bis, Chairman of the CENELEC TC 211 Working Group in charge of mobile and base station standard, and vice chairman of the URSI French commission K. Since 1998, Dr. Wiart is Senior member of the SEE.